Sergey Y. Yurish, Editor

IFSA

Advances in Robotics and Automatic Control: Reviews

1

Advances in Robotics and Automatic Control: Reviews

Book Series, Volume 1

S.Yurish
Editor

Advances in Robotics and Automatic Control: Reviews

Book Series, Volume 1

IFSA International Frequency Sensor Association Publishing

S. Yurish, *Editor*
Advances in Robotics and Automatic Control: Reviews, Book Series, Vol. 1

Published by IFSA Publishing, S. L., 2018,
E-mail (for print book orders and customer service enquires):
ifsa.books@sensorsportal.com

Visit our Home Page on http://www.sensorsportal.com

ISBN: 978-84-09-02449-0
BN-20180530-XX
BIC: TJFM1

Contents

Preface

By 2020 the International Federation of Robotics (IFR) estimates that more than 1.7 million new industrial robots will be installed in factories worldwide and robots for domestic could reach almost 32 million units in the period 2018-2020, with an estimated value of about €10 bn ($11.7 bn).

Industrial robots offer many benefits, including cost reduction, increased rate of operation and improving quality, along with improved manufacturing efficiency and flexibility. The demand for industrial robotics is majorly observed in industries such as automotive, electrical & electronics, chemical, rubber & plastics, machinery, metals, food & beverages, precision & optics, and others. In its turn, industrial automation control market will witness considerable growth during the same period with the growing demand of products such as sensors, drives and various robots.

The first volume of the *Advances in Robotics and Automatic Control: Reviews*, Book Series started by IFSA Publishing in 2018 contains ten chapters written by 32 contributors from 9 countries: Belgium, China, Germany, India, Ireland, Japan, Serbia, Tunisia and USA.

Chapter 1 discusses the electrostatic inchworm motors with low energy consumption using a small size power source. The leg of the microrobot is designed to allow reciprocal motions and powered by Si photovoltaic (hereafter PV) cells.

Chapter 2 describes an adaptive trajectory tracking control for nonholonomic mobile manipulators under modeling uncertainties and external disturbances. One feature of the proposed controller is its model-independent control scheme that can avoid the knowledge of the dynamic parameters and the bound of the external disturbances. Furthermore, the control law is formulated in task space and the redundancy problem is resolved by an extended approach.

Chapter 3 presents a fast approximate nearest neighbor search tree based novelty filter for mobile robotic and video surveillance applications.

Chapter 4 describes control algorithms for the centrifuge flight simulator/spatial disorientation trainer, calculate their kinematic and dynamic parameters in each interpolation period to predict their dynamic behaviour.

Chapter 5 presents state-of-the-art review in the area of continuous hard turning. The various wear mechanisms of polycrystalline cubic boron nitride tool materials are discussed with a view to identifying the critical factors that determine their behaviour in application.

Chapter 6 discusses an approach, which involves factorization of the SLAM posterior over the robot's path, in which each individual particle follows a constant time stereo SLAM approach and the particle distribution is harnessed by the algorithm to estimate the optimal trajectory.

Chapter 7 reports topics in Systems, Control and Optimisation and their evolution through recently funded projects, since about 2013, as well as the EU (e.g. H2020, ERC), National and other Programmes vis-à-vis broader developments.

Chapter 8 summarized a real time switching-model detection Innovation Squared Mismatch (ISM) strategy is presented to enable closed loop control of the switched systems.

Chapter 9 reports H_∞ tracking adaptive fuzzy sliding mode design controller for a class of non square nonlinear systems.

Chapter 10 discusses two formulations of the optimal control problem associated with the optimization of the energy consumed by the induction motor under vector control. The emphasis was placed on the advantage of limiting the control quantities during a real application in order to protect the actuators and the machine.

I hope that readers will enjoy this book and it can be a valuable tool for those who involved in research and development of various robots and automatic control systems.

Sergey Y. Yurish

Editor Barcelona, Spain

Contributors

Riadh Abdelati
University of Monastir, National School of Engineers of Monastir, Tunisia, E-mail: riaabdelati@yahoo.fr

S. Aloui
National Engineering School of Sfax, Laboratory of Sciences and Techniques of Automatic Control & Computer Engineering (Lab-STA), University of Sfax; BP 1173, 3038, Sfax, Tunisia, E-mail: aloui_sinda@yahoo.fr

Mohamed Boukattaya
Laboratory of Sciences and Techniques of Automatic Control & Computer Engineering (Lab-STA), National School of Engineering of Sfax, University of Sfax, Sfax, Tunisia

D. Chatterjee
Indian Statistical Institute, Kolkata, India

Daniel S. Contreras
University of California, Berkeley, USA

M. Elloumi
National Engineering School of Sfax, Laboratory of Sciences and Techniques of Automatic control & computer engineering (Lab-STA), University of Sfax; BP 1173, 3038, Sfax, Tunisia, E-mail: mourad.elloumi@yahoo.fr

Sayan Ghosal
Seagate Technologies LLC, Shakopee, MN, USA

Seamus Gordon
University of Limerick, Plassey, Limerick, Ireland

Minami Kaneko
Nihon University, Tokyo, Japan

Satoshi Kawamura
Nihon University, Tokyo, Japan

Alkis Konstantellos
European Commission, Complex Systems and Advanced Computing Unit Brussels, Belgium

Y. Koubaa
National Engineering School of Sfax, Laboratory of Sciences and Techniques of Automatic Control & Computer Engineering (Lab-STA), University of Sfax; BP 1173, 3038, Sfax, Tunisia, E-mail: Yassine.Koubaa@enis.run.tn

Vladimir Kvrgić
Lola Institute, Kneza Viseslava 70 a, 11030 Belgrade, Serbia

Cora Lahiff
University of Limerick, Plassey, Limerick, Ireland

Liwei Lin
University of California, Berkeley, USA

Yoshio Mita
The University of Tokyo, Tokyo, Japan

Isao Mori
The University of Tokyo, Tokyo, Japan

P. Mukherjee
Department of Computer Science, IIT Kharagpur, Kharagpur, India

S. Patranabis
Department of Computer Science, IIT Kharagpur, Kharagpur, India

Pat Phelan
University of Limerick, Plassey, Limerick, Ireland

Kristofer S. J. Pister
University of California, Berkeley, USA

R. Reiger
Airbus Group HQ HWD1, Germany

Ken Saito
Nihon University, Tokyo, Japan

Murti Salapaka
Department of Electrical and Computer Engineering, University of Minnesota, Twin Cities, USA

A. Sarkar
Department of Mathematics, IIT Kharagpur, Kharagpur, India
Techno India University, Kolkata, India

H. Singh
Department of Computer Science, IIT Kharagpur, Kharagpur, India

Daisuke Tanaka
Nihon University, Tokyo, Japan

Taisuke Tanaka
Nihon University, Tokyo, Japan

Fumio Uchikoba
Nihon University, Tokyo, Japan

Xia Li Wang
Changan University, Xi'an, Shaanxi, China

Xiaochun Wang
Xi'an Jiaotong University, Xi'an, Shaanxi, China

D. Mitchell Wilkes
Vanderbilt University, Nashville, TN, USA

Chapter 1

Electrostatic Inchworm Motors Driven by High-Voltage Si Photovoltaic Cells for Millimeter Scale Multi-Legged Microrobots

Ken Saito, Daniel S. Contreras, Isao Mori, Daisuke Tanaka, Satoshi Kawamura, Taisuke Tanaka, Minami Kaneko, Fumio Uchikoba, Yoshio Mita, Liwei Lin and Kristofer S. J. Pister

1.1. Introduction

Several microrobot systems from the micrometer to centimeter scale have been demonstrated [1-12]. Among these demonstrations, the micrometer scale ones have potential usages in special environments such as surgery inside the narrow blood vessel of a human brain or micro assembly for the small size mechanical system [4, 8] but it is difficult to add power sources and controllers into the microscale system. Therefore, passive control schemes by external electrical or magnetic forces are commonly implemented. On the other hand, a lot of centimeter-size robots have been constructed by the miniaturizations of electrical components with integrated sensors, actuators, power sources and controllers [6, 9]. Despite the fact that multiple bio-inspired robots have been proposed, millimeter scale robots do not perform like insects due to the difficulty in integrating power sources and actuators onto the robot [13-14]. In particular, the locomotion mechanisms of insects attract the attention of researchers [5, 7]. In seeking further miniaturization, some researchers use micro fabrication technology to fabricate small sized actuators [15-16]. For example, piezoelectric actuators, shape memory alloy actuators, electrostatic actuators, ion-exchange polymer actuators, and so on are a few examples. These actuators have different strengths, such as power consumption, switching speed, force generation, displacement, and fabrication difficulty. In general, an actuator can only

Ken Saito
Nihon University, Tokyo, Japan

generate either rotary or linear motion and mechanical mechanisms are necessary to convert the movements generated by the actuators to locomotion.

Previously, the authors have shown a millimeter scale hexapod-type microrobot to perform the tripod gait locomotion of an ant [17], and a quadruped-type microrobot to replicate the quadrupedal gait locomotion of an animal [18] by using shape memory alloy actuators for large deformation and large force. This chapter discusses the electrostatic inchworm motors [19-21] with low energy consumption using a small size power source. The leg of the microrobot is designed to allow reciprocal motions and powered by Si photovoltaic (hereafter PV) cells [22].

1.2. Multi-Legged Microrobot

Fig. 1.1 (a) shows the previous multi-legged microrobot using shape memory alloy type actuator [18]. A previous multi-legged microrobot using shape memory alloy actuator is changed to electrostatic inchworm motors in this work, where each leg of the robot can perform the stepping motion via a single actuator. The leg is fixed on both sides of the body and the microrobot can increase the number of the legs easily. In this chapter, the actuator connection part has been redesigned to accommodate the electrostatic inchworm motors. Fig. 1.1 (b) shows the mechanical parts of the leg made from a silicon wafer except for the shaft and the steady pin. The shapes of the mechanical parts are machined by the inductively coupled plasma dry etching process with photolithography technology. The authors have manual assembled the mechanical parts of the robot because microfabrication technology is hard to construct the complicated three-dimensional structure. In the process, 200 μm-thick silicon wafers were used for the mechanical parts except for the washer which used 100 μm-thick silicon wafers. The shaft was constructed by using 0.1 ± 0.002 mm in diameter cemented carbide. The washer was mounted to the end of a shaft to fix the silicon parts. To keep the parts rigidly connected, the washer and the shaft were glued using cyanoacrylate. All silicon parts have a clearance of a 10 μm gap with respect to the other fitted parts. Since these actuators can only generate the rotary motion or linear motion, linkage assemblies are needed for a microrobot to move using the stepping pattern. The stepping pattern realized by two sets of four-bar linkages. Bar 1, bar 2, bar 5 and bar 6 are the primary (top) four-bar linkage. Bar 3, bar 4, bar 5 and bar 6 are the secondly (bottom) four-bar linkage. The primarily four-bar linkage and secondly four-bar linkage are combined with each other with bar 5 and bar 6 (Fig. 1.1 (c)).

Fig. 1.2 shows the leg motion and trajectory of the leg. The inflection point of the trajectory has four points such as (x_1, y_1), (x_2, y_2), (x_3, y_3) and (x_4, y_4). The steady pin and the hole of bar 5 cause the inflection of the trajectory. The four points can be expressed by the difference of angles of θ_A and θ_{Foot}. The difference of θ_A and θ_{Foot} can perform the reciprocal movement of point P. In other words, Fig. 1.2 shows that the designed leg can perform the stepping motion by the reciprocal movement of point P.

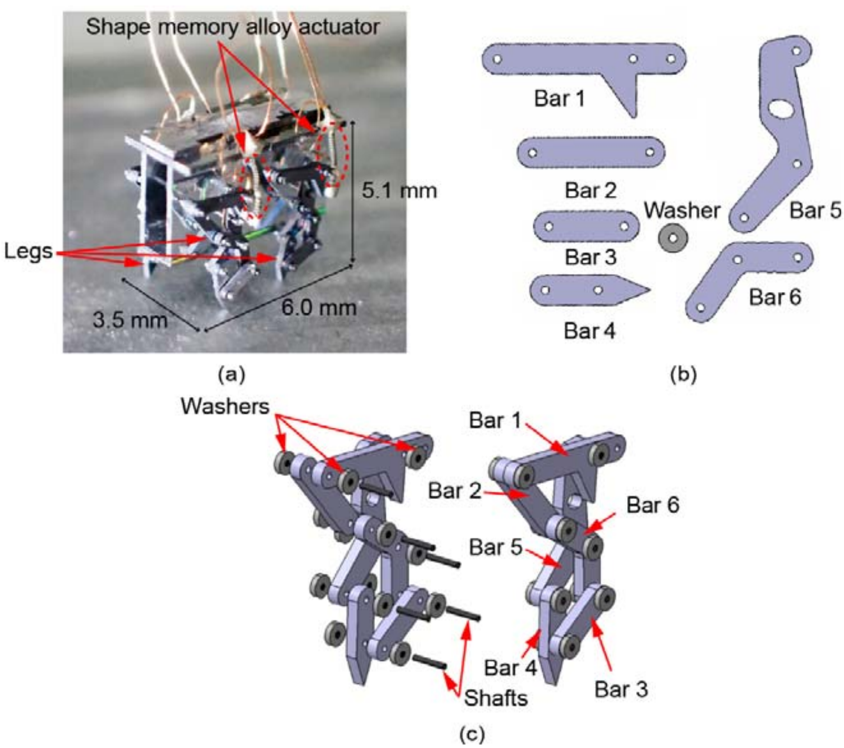

Fig. 1.1. (a) Previous multi-legged microrobot using shape memory alloy type actuator [18]. Mechanical parts of the leg for microrobot with (b) individual parts; (c) assembled structure.

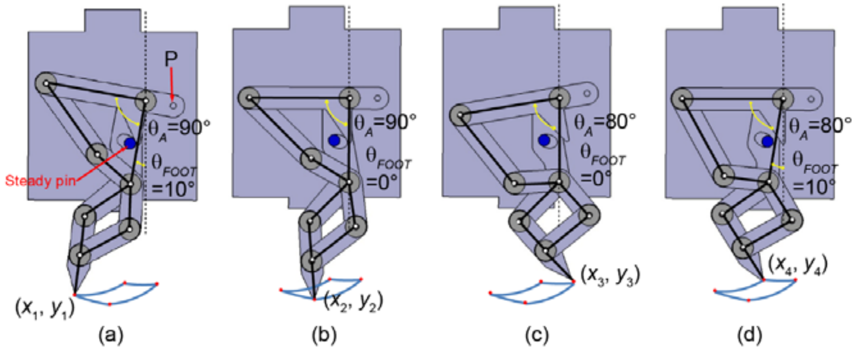

Fig. 1.2. Leg motion and trajectory of the leg. (a) (x_1, y_1) at θ_A=90°, θ_{FOOT}=10°; (b) (x_2, y_2) at θ_A=90°, θ_{FOOT}=0°; (c) (x_3, y_3) at θ_A=80°, θ_{FOOT}=0°; (d) (x_4, y_4) at θ_A=80°, θ_{FOOT}=10°.

The authors design the mechanical parts of the leg according to the mathematical equations. Fig. 1.3 and Table 1.1 show the conditions to describe the point of the leg (x_n, y_n). The (x_0, y_0) is the origin coordinate which is the only fixed point of the robot. The upper case alphabet A, B, C, D, E, F, G, H and I show the name of each lengths. L1 and L3 show the auxiliary lines from (x_0, y_0) to bar 4 which is the bar contains the point of the leg. θ_3, θ_5, θ_7, θ_B and θ_{A0} are described as Fig. 1.3 (b).

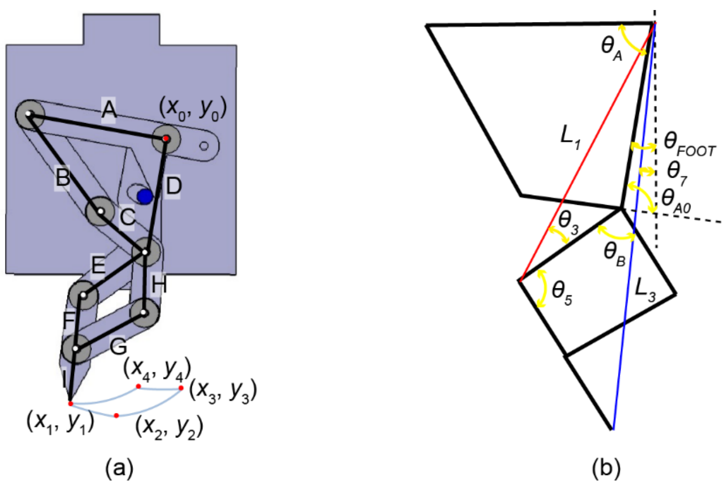

Fig. 1.3. Name of each bars, coordinates and angles of the leg. (a) Length and coordinates; (b) Angles and auxiliary lines.

Table 1.1. Length between the node points.

Name of bar	Name	Length (μm)
Bar 1	A	1800
Bar 2	B	1556
Bar 6	C	800
Bar 5	D	1500
Bar 5	E	1000
Bar 4	F	700
Bar 3	G	1000
Bar 6	H	800
Bar 4	I	700

The (x_n, y_n) (n=1, 2, 3, 4) can describe by the Equation (1.1):

$$(x_n = L_3 \cos(-90° - \theta_7 - \theta_{Foot}), y_n = L_3 \sin(-90° - \theta_7 - \theta_{Foot})), \quad (1.1)$$

where θ_7, L_3, L_1, θ_5, θ_3, θ_B and θ_{A0} are the following Equation (1.2), (1.3), (1.4), (1.5), (1.6), (1.7) and (1.8), respectively.

$$\theta_7 = \cos^{-1}\frac{{L_1}^2+D^2-E^2}{2L_1D} - \cos^{-1}\frac{{L_1}^2+{L_3}^2-(F+I)^2}{2L_1L_3}, \quad (1.2)$$

$$L_3 = \sqrt{{L_1}^2 + (F+I)^2 - 2L_1(F+I)\cos(\theta_3+\theta_5)}, \quad (1.3)$$

$$L_1 = \sqrt{D^2 + E^2 - 2D^2\cos 135°}, \quad (1.4)$$

$$\theta_5 = \cos^{-1}\left(\frac{E - H\cos\theta_B}{\sqrt{E^2+H^2-2EH\cos\theta_B}}\right) + \\ +\cos^{-1}\left(\frac{E^2+H^2-G^2+F^2-2EH\cos\theta_B}{2F\sqrt{E^2+H^2-2E\cos\theta_B}}\right), \quad (1.5)$$

$$\theta_3 = 180° - \left(135° + \cos^{-1}\frac{{L_1}^2+D^2-E^2}{2L_1D}\right), \quad (1.6)$$

$$\theta_B = 360° - (\theta_{A0} + 135° + 50°), \quad (1.7)$$

$$\theta_{A0} = 180° - \left(\cos^{-1}\left(\frac{D - A\cos\theta_A}{\sqrt{D^2+A^2-2DA\cos\theta_A}}\right) + \\ +\cos^{-1}\left(\frac{D^2+A^2-B^2+C^2-2DA\cos\theta_A}{2C\sqrt{D^2+A^2-2DA\cos\theta_A}}\right)\right), \quad (1.8)$$

Table 1.2 shows the derived coordinates of the each foot point using the above equations and conditions. This result shows the designed leg can perform the stepping motion which is needed to move the multi-legged microrobot.

Table 1.2. Coordinates of each foot point.

Foot point	θ_A and θ_{Foot}	Coordinates
(x_1, y_1)	90° and 10°	(-1248.6, -3440.3)
(x_2, y_2)	90° and 0°	(-632.3, -3604.9)
(x_3, y_3)	80° and 0°	(227.2, -3249.4)
(x_4, y_4)	80° and 10°	(-340.5, -3239.5)

Fig. 1.4 shows the measurement method for the required force F_S to actuate the leg. The required force can describe by the Equation (1.9):

$$F_s = M_W\,g, \qquad (1.9)$$

where M_W is the mass of the weight and g is the gravity acceleration. The authors vary the mass of the weight to find the minimum weight to actuate the leg. Fig. 1.4(a) is the required force for the push motion.

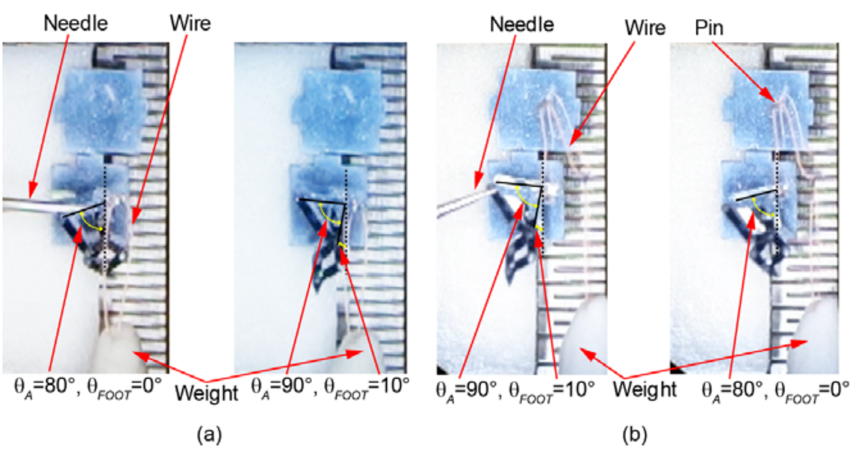

Fig. 1.4. Measurement method for the required force to actuate the leg for (a) push motion; (b) pull motion.

The weight was attached to point P of bar 1 using a wire. The required force of 542 μN is measured in order to move the leg to the regular position under the lightest weight of 55.3 mg. Fig. 1.4 (b) shows the required force for the pull motion. The weight was attached to the point P of bar 1 using a wire through the pin and the lightest weight was 36.2 mg, while the force for this pull motion was 355 μN.

1.3. Electrostatic Inchworm Motors

As an alternative low-power means of actuation, electrostatic inchworm motors can be used to drive the legs of the microrobot. MEMS electrostatic inchworm motors are based on capacitively driven gap-closing actuators (GCA) working in tandem to displace a shuttle linearly at over 100 μN force output without any static current [19].

The authors used an angled-arm design based on work from [20]. In this design, the GCAs use an attached angled-arm to impact a central shuttle and move it in a preferential direction. The motors have a gap size of 2.1 μm and each step of the motor moves the shuttle by 1 μm. Each GCA has 70 fingers, totalling 140 fingers for each actuation step. The inchworm motor chiplet measures a total area of approximately 2.2 mm × 2.5 mm. The electrostatic inchworm motors are fabricated in a 3-mask silicon-on-insulator (SOI) process. The SOI wafers had a 40 μm device layer, 2 μm buried oxide and 550 μm handle wafer. A layer of 100 nm-thick aluminium is deposited on the device-layer silicon to define the contact pads. The device layer silicon is etched to form the structure of the motors using DRIE. A backside etch is then performed to reduce the mass and release the singulated chiplets from the substrate.

Fig. 1.5 shows the force output of an electrostatic inchworm motor. Force measurements are taken using a serpentine spring assembly attached to the motor shuttle. The serpentine assembly has a spring constant of 18.5 N/m. By measuring the displacement of the inchworm shuttle, we can relate this to the force output of the motor. The solid line highlights the analytical calculation of the force output. We can see that at 60 V we get an average force output of over 1 mN from 5 measured devices. The original angled-arm inchworm motors shown in [20] were able to generate 1.88 mN at 110 V. Previous work has shown 500 μN of force at 60 V [21] while the newly fabricated devices have demonstrated 1 mN of force at 60 V. Discrepancies between the analytical model and the measured values can be attributed to unaccounted lateral etching of the silicon sidewalls. This can increase the effective finger gap size and change the spring constants of the springs.

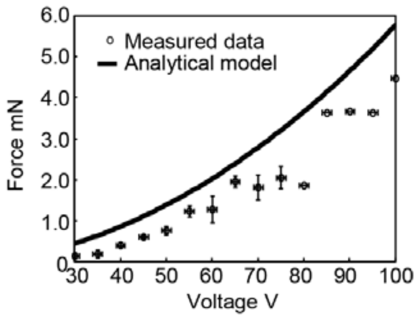

Fig. 1.5. The raw force output of the inchworm motor used in these experiments.

1.4. High-Voltage Si PV Cells

Fig. 1.6 shows the fabricated high-voltage Si PV cell array. The PV cell array was designed in an area of about 3 mm square. The device was made by CMOS post-process dry release and device isolation method. The array consists of 125 PV cells connected in series and each cell has a p-diffusion layer on n-well. The details of the design and process method are shown in reference [22].

In the reference [22], the light source of the PV cell array was a red LED with 30 mA current. The open circuit voltage (VOC) was 57.9 V, from which we can deduce that the open circuit voltage of each cell was about 0.46 V on average. The short circuit current (ISC) was 976 nA. The maximum power (Pmax) was 43.3 μW, where the voltage was 53.2 V and the current was 683 μA. The fill factor (FF; FF = Pmax/VOC ISC) was 76.7 %. The FF generally indicates the quality of the pn-junctions (a high fill factor means a high quality of the junction) and the value 76.7 % is relatively high. This high value was achieved by using a commercial CMOS process performed by a foundry. However, the maximum power in the reference [22] was not high enough to actuate the electrostatic inchworm motors. The authors changed the light source to a xenon lamp with 5 A current to achieve VOC=60.0 V and ISC=105 μA. Fig. 1.7 shows the I-V characteristics of the PV cell array lighted with the xenon lamp. The xenon lamp irradiated the PV cell from a distance of 10 cm. This result shows that the xenon lamp can produce 30 times the power shown in the reference [22], large enough to actuate the electrostatic inchworm motors.

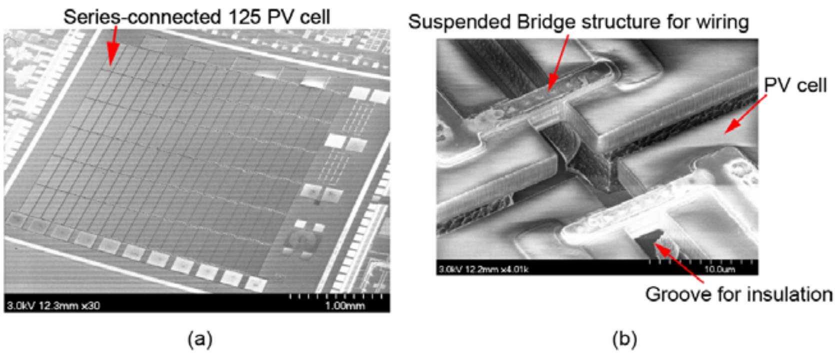

Fig. 1.6. Fabricated PV cell array [22]. (a) Whole view; (b) Magnified view.

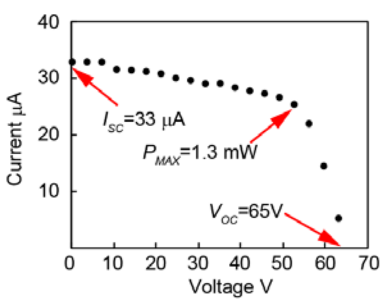

Fig. 1.7. I-V curve of 125-cell PV array (Light source: xenon lamp).

1.5. Experimental Results

Fig. 1.8(a) shows an inchworm motor chip. The image highlights the ring meant to engage to a complimentary post on the leg, the gap closing actuators, the reset spring, and the signal pads that receive signals from the drive circuit. The inchworm motor is fabricated in the 3-mask process described in Section 1.3. This motor has the force profile shown in Fig. 1.5. Fig. 1.8 (b) highlights the methodology of integration of the inchworm chip with the leg. The motor is taped onto a platform off of a micromanipulator stage. This is because aligning the ring with the post and interfacing the parts require careful precision. Once the leg engagement ring is in place on the leg post, a set of probes are dropped onto the motor contact pads to provide the electrical signals from the circuit needed to drive the motor. This circuit is powered by the solar cell.

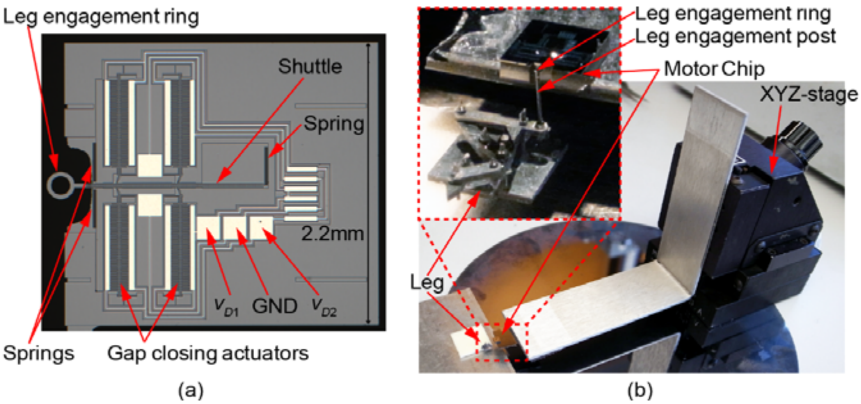

Fig. 1.8. Details of the inchworm motor chip integration (a) A micrograph of the motor chip highlighting the leg engagement ring, gap closing actuators, shuttle, spring, and the electrical contact pads. The pads are driven with probes that are connected to the circuit that is driven by the solar cells; (b) A diagram of the experimental setup showing the leg engagement post, meant to interface with the leg engagement ring. The motor chip is held on a platform on a micromanipulator stage and the ring is maneuvered around the post. Once the motor is in place, the probes are dropped onto the motor chip to drive the leg.

Fig. 1.9 shows the actuation experimental setup of the electrostatic inchworm motors using PV cell array (Fig. 1.9 (a)). The anode-side of PV cell array was connected to the solid resistor at the collector of the transistor. In other words, the generated voltage by the PV cell, V_{PV}, was used as the voltage source of the circuit. The Arduino was used for switching the transistor for generating the driving waveform v_{D1} and v_{D2} for the electrostatic inchworm motors (Fig. 1.9(b)). The driving waveforms were two offset 60 V amplitude 500 Hz square waves, one for each of the GCAs of the motor.

Fig. 1.10 shows the generated force of the electrostatic inchworm motors. The force gauge system was attached on the shuttle and the scale of the force gauge was characterized as 1 dot = 0 μN, 2 dot = 370 μN, 3 dot = 740 μN. The guideline is attached to the shuttle to point the dot. The result in Fig. 1.11 shows that the guideline points the 3 dot. This result shows the generated force was 740 μN according to the gauge system, which is high enough to actuate the leg of the microrobot.

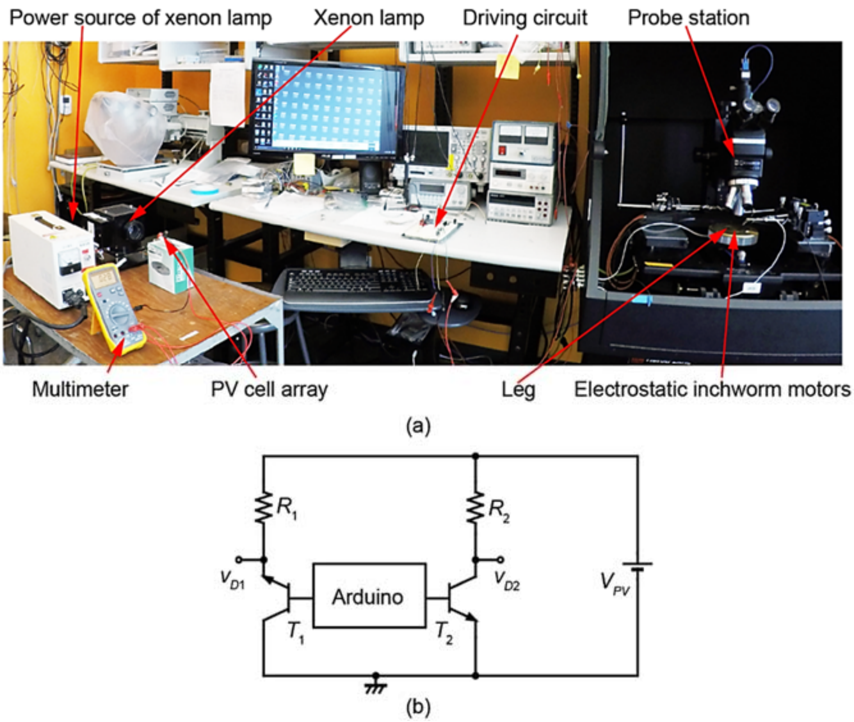

Fig. 1.9. Actuation experimental setup: (a) Whole setup; (b) Circuit diagram of driver circuit.

Fig. 1.11 shows the actuation of the leg using electrostatic inchworm motors. The ring structure was attached to the shuttle of the electrostatic inchworm motors using the method described above. The electrostatic inchworm motors was connected to the leg through the shaft of point P. The result in Fig. 1.11 shows that the electrostatic inchworm motors produced about 250 μm in displacement to move the leg of the microrobot. However, the pull motion was not enough to actuate the leg from (x_4, y_4) to (x_1, y_1). This is because spring was designed to generate the 250 μN pull motion. The pull motion needs 355 μN to complete the motion. The strength of the spring needs for the future examination.

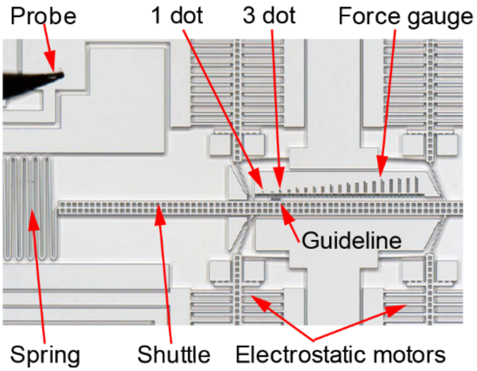

Fig. 1.10. Generated force measurement of the electrostatic inchworm motors.

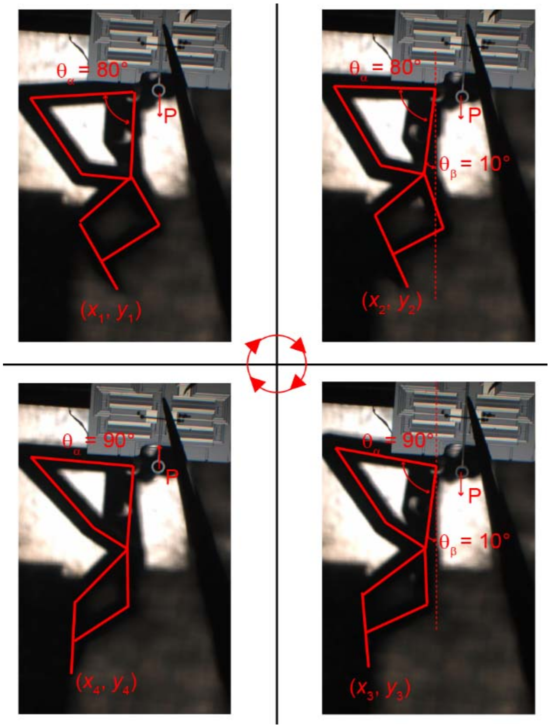

Fig. 1.11. Actuation of leg: (a) Pull motion; (b) Push motion.

1.6. Conclusions

In this chapter, the electrostatic actuator with low energy consumption is powered by a 3 mm × 3 mm Si photovoltaic cells with an output voltage of 60 Volts. The generated force of the electrostatic inchworm motors was 740 μN to actuate the leg of the microrobot. The leg of the microrobot could move using the electrostatic inchworm motors with proper driving waveforms for large displacements. In the future, the authors will design the millimeter scale locomotive robot with Si PV cell driven electrostatic inchworm motors.

Acknowledgements

The fabrication of the microrobot was supported by Research Center for Micro Functional Devices, Nihon University. Fabrication of the inchworm motors was supported by the UC Berkeley Marvell Nanofabrication Laboratory. The authors would like to acknowledge the Berkeley Sensor and Actuator Center and the UC Berkeley Swarm Lab for their continued support. VLSI Design and Education Center (VDEC), the University of Tokyo (UTokyo) and Phenitec Semiconductor are acknowledged for CMOS-SOI wafer fabrication. Japanese Ministry of Education, Sports, Culture, Science and Technology (MEXT) is acknowledged for financial support through Nanotechnology Platform to UTokyo VDEC used for PV cell post-process.

References

[1]. Ebefors T., Mattsson J. U., Kälvesten E., Stemme G., A Walking Silicon Micro-robot, in *Proceedings of the 10th Int. Conference on Solid-State Sensors and Actuators (TRANSDUCERS' 99)*, Sendai, Japan, 1999, pp. 1202-1205.

[2]. Hollar S., Flynn A., Bellew C., Pister K. S. J., Solar powered 10 mg silicon robot, in *Proceedings of the IEEE Sixteenth Annual International Conference on Micro Electro Mechanical Systems*, Kyoto, Japan, 2002, pp. 706-711.

[3]. Ryu J., Jeong Y., Tak Y., Kim B., Kim B., Park J., A ciliary motion based 8-legged walking micro robot using cast IPMC actuators, in *Proceedings of the International Symposium on Micromechatronics and Human Science*, 2002, pp. 85-91.

[4]. Donald B. R., Levey C. G., McGray C. D., Paprotny I., Rus D., An Untethered, Electrostatic, Globally Controllable MEMS Micro-Robot, *Journal of Microelectromechanical Systems*, Vol. 15, No. 1, 2006, pp. 1-15.

[5]. Hoover M. A., Steltz E., Fearing S. R., RoACH: An autonomous 2.4 g crawling hexapod robot, in *Proceedings of the IEEE/RSJ International Conference on Intelligent Robots and Systems*, Nice, France, 22–26 September 2008, pp. 26–33.

[6]. Kernbach S., Kernbach O., Collective energy homeostasis in a large-scale microrobotic swarm, *Robotics and Autonomous Systems*, Vol. 59, 2011, pp. 1090-1101.

[7]. Wood R. J., Finio B., Karpelson M., Ma K., Pérez-Arancibia N. O., Sreetharan P. S., Tanaka H., Whitney J. P., Progress on "Pico" Air Vehicles, *The International Journal of Robotics*, Vol. 31, No. 11, 2012, pp. 1292-1302.

[8]. Donald B. R., Levey C. G., Paprotny I., Rus D., Planning and control for microassembly of structures composed of stress-engineered MEMS microrobots, *The International Journal of Robotics Research*, Vol. 32, No. 2, 2013, pp. 218–246.

[9]. Rubenstein M., Cornejo A., Nagpal R., Programmable self-assembly in a thousand-robot swarm, *Science*, Vol. 345, No. 6198, 15 Aug. 2014, pp. 795-799.

[10]. Jinhong Qu J., Oldham K. R., Multiple-Mode Dynamic Model for Piezoelectric Micro-Robot Walking, in *Proceedings of the 21st Design for Manufacturing and the Life Cycle Conference and 10th International Conference on Micro- and Nanosystems*, Vol. 4, 2016, Paper No. DETC2016-59621.

[11]. Vogtmann D., Pierre R. S., Bergbreiter S., A 25 MG Magnetically Actuated Microrobot Walking at > 5 Body Lengths/sec, in *Proceedings of the IEEE 30th International Conference on Micro Electro Mechanical Systems*, Las Vegas, NV, USA, 2017, pp. 179-182.

[12]. Rahmer J., Stehning C., Gleich B., Spatially selective remote magnetic actuation of identical helical micromachines, *Sci. Robot.*, Vol. 2, 2017.

[13]. Abbott J. J., Nagy Z., Beyeler F., Nelson B. J., Robotics in the Small, Part I: Microbotics, *IEEE Robotics & Automation Magazine*, Vol. 14, No. 2, 2007, pp. 92-103.

[14]. Cho K., Wood R., Biomimetic robots, *Springer International Publishing*, Cham, Switzerland, Chap. 23, 2016.

[15]. Fearing R. S., Powering 3 Dimensional Microrobots: Power Density Limitations, in *Proceedings of the IEEE International Conference on Robotics and Automation, Tutorial on Micro Mechatronics and Micro Robotics*, 1998.

[16]. Bell D. J., Lu T. J., Fleck N. A., Spearing S. M., MEMS actuators and sensors: observations on their performance and selection for purpose, *Journal of Micromechanics and Microengineering*, Vol. 15, No. 7, 2005, pp. S153-S164.

[17]. Saito K., Maezumi K., Naito Y., Hidaka T., Iwata K., Okane Y., Oku H., Takato M., Uchikoba F., Neural Networks Integrated Circuit for Biomimetics MEMS Microrobot, *Robotics*, Vol. 3, 2014, pp. 235-246.
[18]. Tanaka D., Uchiumi Y., Kawamura S., Takato M., Saito K., Uchikoba F., Four-leg independent mechanism for MEMS microrobot, *Artificial Life and Robotics*, Vol. 22, No. 3, September 2017, pp 380–384.
[19]. Yeh R., Hollar S., Pister K. S. J., Single mask, large force and large displacement electrostatic linear inchworm motors, *Journal of Microelectromechanical Systems*, Vol. 11, No. 4, 2002, pp. 330-336.
[20]. Penskiy I., Bergbreiter S., Optimized electrostatic inchworm motors using a flexible driving arm, *Journal of Micromechanics and Microengineering*, Vol. 23, No. 1, 2012, pp. 1-12.
[21]. Contreras D. S., Drew D. S., Pister K. S. J., First steps of a millimeter-scale walking silicon robot, in *Proceedings of the 19th Int. Conference on Solid-State Sensors, Actuators and Microsystems*, Kaohsiung, Taiwan, 2017.
[22]. Mori I., Kubota M., Lebrasseur E., Mita Y., Remote power feed and control of MEMS with 58 V silicon photovoltaic cell made by a CMOS post-process dry release and device isolation method, in *Proceedings of the Symposium on Design, Test, Integration & Packaging of MEMS/MOEMS (DTIP'14)*, Cannes, France, 1-4 April 2014.

Index

D

E

F

G

H

I

J

K

L

M

N

O

P

Q

R

S

T

U

V

W

X

IFSA

Advances in Robotics and Automatic Control: Reviews Volume 1

Sergey Y. Yurish, Editor

Industrial robots offer many benefits, including cost reduction, increased rate of operation and improving quality, along with improved manufacturing efficiency and flexibility. The demand for industrial robotics is majorly observed in industries such as automotive, electrical & electronics, chemical, rubber & plastics, machinery, metals, food & beverages, precision & optics, and others. In its turn, industrial automation control market will witness considerable growth during the same period with the growing demand of products such as sensors, drives and various robots.

The first volume of the *'Advances in Robotics and Automatic Control: Reviews'*, Book Series started by IFSA Publishing in 2018 contains ten chapters written by 32 contributors from 9 countries: Belgium, China, Germany, India, Ireland, Japan, Serbia, Tunisia and USA.

This book will be a valuable tool for those who involved in research and development of various robots and automatic control systems.

ISBN 978-84-697-3467-4

9 788469 734674